Synergistic effect between copper and cerium on the performance of Cu$_x$-Ce$_{0.5-x}$-Zr$_{0.5}$ (x = 0.1–0.5) oxides catalysts for selective catalytic reduction of NO with ammonia

Sher Ali, Liqiang Chen, Fulong Yuan, Rui Li, Tianrui Zhang, Syed ul Hasnain Bakhtiar, Xuesong Leng, Xiaoyu Niu*, Yujun Zhu*

Key Laboratory of Functional Inorganic Material Chemistry (Heilongjiang University), Ministry of Education, School of Chemistry and Materials, Heilongjiang University, Harbin, 150080 PR China

ABSTRACT

A series of Cu$_x$-Ce$_{0.5-x}$-Zr$_{0.5}$ oxides catalysts with different Cu/Ce ratio were synthesized by citric acid method. The catalysts were characterized by XRD, BET surface area, H$_2$-TPR, NH$_3$-TPD, NO-TPD, XPS and *in-situ* DRIFTS. The synergistic effect between copper and cerium on the catalytic performance of Cu$_x$-Ce$_{0.5-x}$-Zr$_{0.5}$ for selective catalytic reduction of NO with ammonia was investigated. It was found that the Cu$_{0.2}$-Ce$_{0.3}$-Zr$_{0.5}$ catalyst show the excellent SCR activity, N$_2$ selectivity and H$_2$O/SO$_2$ durability in a low temperature range of 150–270 °C even at high gas hourly space velocity of 84,000 h^{-1}. The strong interaction leads to the improvement of the acidity and the increase in the amount of active oxygen species (oxygen vacancy), which are responsible for the higher activity at low temperatures. The SCR reaction process over Cu$_{0.2}$-Ce$_{0.3}$-Zr$_{0.5}$ was also examined using *in-situ* DRIFTS. The DRIFTS results indicate that abundant ionic NH$_4^+$ (Brønsted acid sites), coordinated NH$_3$ on the Lewis acid sites, as well as highly active monodentate nitrate and bridging nitrate species were the key intermediates in the SCR reaction.

© 2017 Elsevier B.V. All rights reserved.

1. Introduction

Nitrogen oxides (NO$_x$) are the major contributors to certain environmental issues such as air pollutant, acid rain, ozone depletion, photochemical smog and global warming [1–7]. The emission of NO$_x$ to the atmosphere derives from stationary source such as different coal fired power plants and mobile source such as motor vehicle. Rigorous emission control standards, stringent emission regulations and increasing environmental awareness are being imposed or raised for the abatement of NO$_x$ pollution from the atmosphere [8]. To get this task, efficient denitrification has become a very imperative, effective, interesting and challenging research area worldwide. Different denitrification techniques such as electron beam irradiation, pulse corona plasma, carbon reduction, adsorption method, selective non-catalytic reduction, selective catalytic reduction (SCR) and so on have been studied in recent years for NO$_x$ removal from the stationary sources [6,7,9]. Among all these denitrification techniques, SCR at low temperatures has been known as the most promising commercial technique for removing NO$_x$ [8,10,11], especially from cement and steel manufacture.

One of the most commercially used catalysts is V$_2$O$_5$-WO$_3$(MoO$_3$)-TiO$_2$ [2,9,12]. But certain limitations constrain their usage, for example, it is active within a relatively narrow operation temperature window of 300–400 °C and vanadium toxicity. Consequently, it is very important to develop novel low temperature NH$_3$-SCR catalysts with high N$_2$ selectivity and good activity especially below 300 °C [2]. In recent years, many transitional metal oxides including NiO, FeO$_x$, MnO$_x$, CeO$_2$, CuO$_x$ and a wide range of mixed metal oxides [2,4,13–16] have been reported as effective catalysts for low-temperature NH$_3$-SCR of NO reaction. The Cu containing catalysts mostly presented in the form of Cu exchanged zeolites such as Cu/SAPO-34, which displayed excellent low temperature activity [17]. But due to the high cost of the Cu/SAPO-34, the Cu containing mixed metal oxide catalysts were prepared. CuO$_x$ impregnated on the co-precipitated WO$_3$-ZrO$_2$ support displayed better ammonia adsorption, which was essential for high SCR activity, and also exhibited 100% NO$_x$ conversion in the range of 200–320 °C [16]. According to the Sullivan et al. [18], the Cu containing catalyst synthesized from two different precursors (Cu(NO$_3$)$_2$ and CuSO$_4$) with numerous oxide supports (TiO$_2$, Al$_2$O$_3$ and SiO$_2$)

---

* Corresponding author.
E-mail addresses: niuxiaoyu@hlju.edu.cn (X. Niu), yujunzhu@hlju.edu.cn, yujunzhu@126.com (Y. Zhu).

were also active in the NH$_3$-SCR reaction, and exhibited excellent NO$_x$ conversion in a wide temperature window.

Ceria is very famous for their high redox ability via Ce^{4+} to Ce^{3+} transition and outstanding oxygen storage capacity [19–21]. Due to these properties, Ce has been extensively studied as an active component in the SCR reaction. However, pure CeO$_2$ displays poor thermal stability because of the susceptible sintering property at high temperature. In order to overcome these deficiencies and increase its thermal stability and ability to store and release oxygen throughout high temperature reaction, other transition and non-transition metal ions can be introduced into the ceria cubic structure [20]. The CeO$_2$-TiO$_2$ catalysts were reported to possess excellent catalytic activity, high tolerance to SO$_2$ and H$_2$O and high N$_2$ selectivity in the NH$_3$-SCR reaction [22–24]. In our previous study [25], we found the complete amorphous Ce$_{0.3}$TiO$_x$ catalyst demonstrated excellent catalytic performance for NH$_3$-SCR of NO, which was associated with the strong interactions between Ce and Ti, higher BET surface area, abundant acid sites, presence of abundant Ce^{3+} and chemisorbed oxygen. The low-cost and easy combination of ceria and copper oxide can provide novel catalysts with excellent H$_2$O/SO$_2$ resistance, N$_2$ selectivity and low-temperature activity [26,27]. Guo et al. [28] reported that CuO-CeO$_2$ catalyst displayed outstanding low temperature SCR activity, and furthermore it was concluded that the state of Cu species had great influence on the SCR activity. According to the studies by Iang et al. [29], CuO-CeO$_2$ supported on carbon fiber displayed high activity for urea-SCR of NO at room temperature. Gao

et al. [30] reported that the Ce-Cu-Ti catalyst showed outstanding performance even in the presence of H$_2$O and SO$_2$. Many other catalysts such as CuO/WO$_3$/Ce$_{0.5}$Zr$_{0.5}$O$_2$ [31], CuO/CeO$_2$/ZrO$_2$ [32] and CuO-CoO$_x$/Ce$_{0.67}$Zr$_{0.33}$O$_2$ [33], also displayed excellent NH$_3$-SCR reaction activities in the temperature range of 200–450 °C.

It has been reported that the addition of ZrO$_2$ to CeO$_2$ can improve the thermal stability and oxygen storage capacity [34]. In addition, we also found more Cu$^+$ and highly dispersed copper oxide species can be formed in the CuO-Ce$_{0.9}$Zr$_{0.1}$O$_2$ catalysts, which would be favor of NH$_3$-SCR reaction [35]. To the best of our understanding, little is known about the effects of interaction between copper and cerium on zirconia, which may play a vital role in enhancing dispersion of copper and improving NO/NH$_3$ adsorptive properties of catalysts. The synergistic effects between copper oxide and cerium oxide on the redox properties and the adsorption behavior of catalysts may help to further understand the reaction mechanism.

In this work, a series of Cu$_x$-Ce$_{0.5-x}$-Zr$_{0.5}$ ($x = 0.1, 0.2, 0.3, 0.4, 0.5$) catalysts was prepared by citric acid method and was used for NH$_3$-SCR of NO. The synergistic effect between Cu and Ce oxides on the performance of Cu$_x$-Ce$_{0.5-x}$-Zr$_{0.5}$ catalysts for NH$_3$-SCR of NO was investigated. The Cu$_{0.2}$-Ce$_{0.3}$-Zr$_{0.5}$ catalyst showed excellent catalytic performance and SO$_2$/H$_2$O resistance for the SCR of NO with NH$_3$. We paid specially attention to the process of the SCR reaction and the SO$_2$ poisoning of the Cu$_{0.2}$-Ce$_{0.3}$-ZrO$_2$ by in situ diffuse reflectance infrared Fourier transform spectroscopy (DRIFTS).
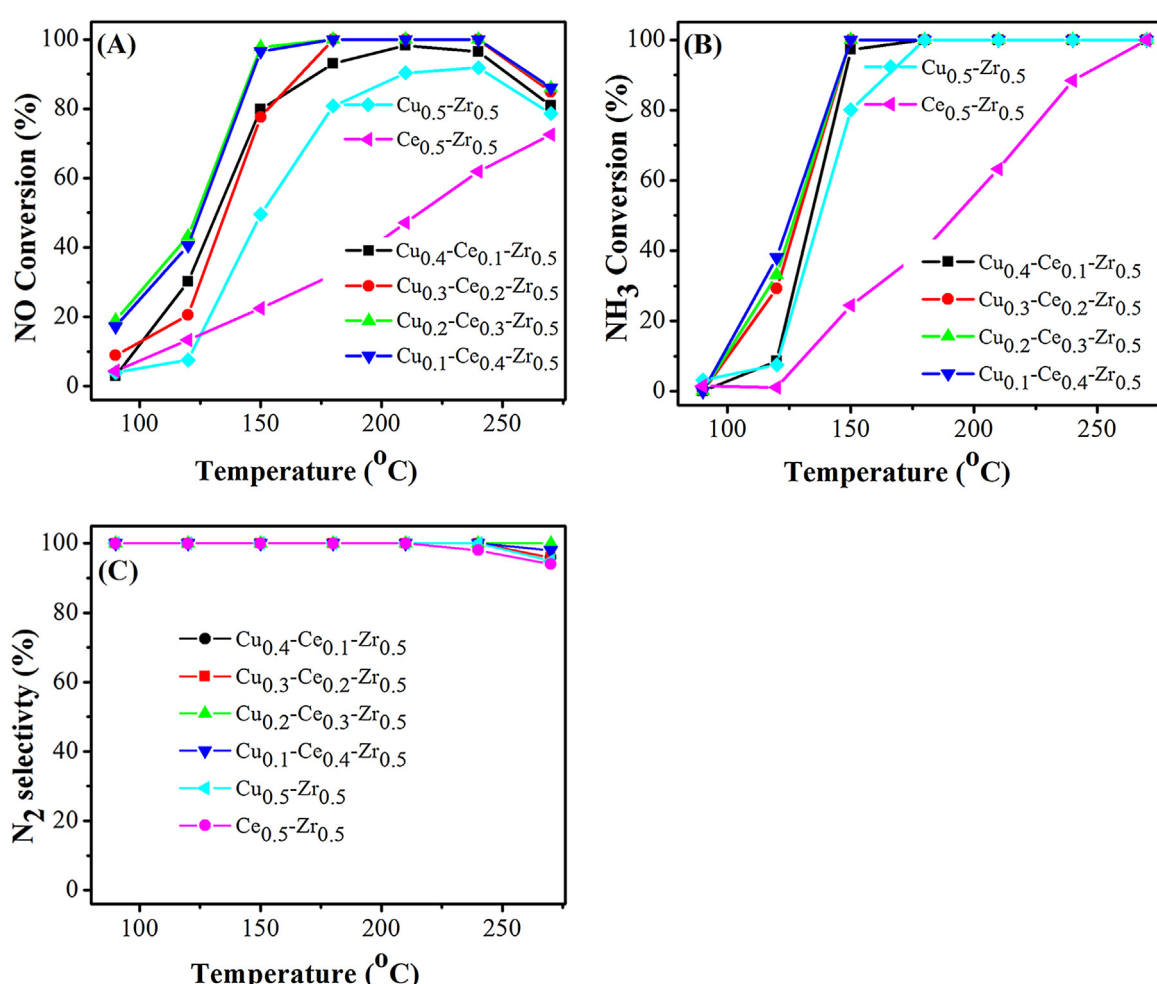

Fig. 1. (A) NO$_x$ conversion, (B) NH$_3$ conversion (C) N$_2$ selectivity over the Cu$_x$-Ce$_{0.5-x}$-Zr$_{0.5}$ ($x = 0$–0.5) catalysts as a function of temperature (Reaction conditions: [NO] = [NH$_3$] = 1000 ppm, [O$_2$] = 3%, N$_2$ balances, GHSV = 28,000 h^{-1}).

2. Experimental

2.1. Catalyst preparation

The Cu_x-$Ce_{0.5-x}$-$Zr_{0.5}$ (x = 0.1, 0.2, 0.3, 0.4) catalysts were prepared by the citric acid method. Zirconium nitrate (0.5 mol), cupric nitrate (0.1-0.4 mol) and cerium nitrate hexahydrate (0.1–0.4 mol) were mixed in designated ratios and added to aqueous citric acid (1.0 mol) solution (50 mL). The molar ratio of the total metal components (the sum of Cu, Ce and Zr) to citric acid was kept to 1.0:1.0. The resultant mixtures were stirred at room temperature until complete dissolution of the salts. The solution was then dried at 120 °C for 10 h resulting in porous foam like solid. This precursor was calcined at 500 °C for 5.0 h in air in muffle furnace. Finally, the samples were crushed and sieved to 40–60 mesh prior to use for evaluating catalytic activity. $Cu_{0.5}$-$Zr_{0.5}$ and $Ce_{0.5}$-$Zr_{0.5}$ (Cu_x-$Ce_{0.5-x}$-$Zr_{0.5}$ (x = 0 and 0.5)) as references were also prepared according to above method.

2.2. Characterizations

The X-ray diffraction (XRD) patterns were obtained using a Bruker D8 Advance X-ray diffractometer with Cu Kα (λ = 1.5418 Å) radiation (40 kV, 40 mA). The data were collected in the 2θ range of 20–80° with the steps of 0.02°. The BET surface area was measured by Micromeritics Tristar II analyzer at liquid N_2 temperature (−196 °C). The Temperature Programed Reduction (H_2-TPR) experiment was carried out through AutoChem TP5080 chemisorptions analyzer (Xianquan Tianjin, China). In the typical TPR experiment, firstly, 0.020 g sample was pretreated under O_2 stream (25 mL/min) for 1 h at 300 °C, and cooled down to room temperature in the same stream. Then, the sample was heated to 800 °C at a heating rate of 10 °C/min in a 5% H_2/N_2 flow (30 mL/min). Temperature programmed desorption of NH_3/NO (NH_3-TPD and NO-TPD) studies were carried out by using the AutoChem TP5080 chemisorptions analyzer, and using mass spectra (QIC-20, Hidden) to record the signals of NH_3 (m/z = 17), N_2O (m/z = 44), N_2 (m/z = 28), O_2 (m/z = 32) or NO_2 (m/z = 46). In the NH_3-TPD and NO-TPD experiments, 0.100 g of catalyst was pretreated in helium stream at 300 °C for 1 h. Then, the sample was cooled down to room temperature in the same helium stream. In the second step, the catalyst was saturated with anhydrous NH_3 (0.8% NO/N_2) at a flow rate of 30 mL/min for 1 h, followed by helium (30 mL/min) purging for 1 hour to purge the physically absorbed NH_3/NO. Finally, the sample was heated from room temperature to 400 °C (NH_3-TPD)/500 °C (NO-TPD) at a rate of 10 °C/min under a He flow of 30 mL/min. X-ray photoelectron spectroscopy (XPS) experiment was performed by a Kratos-AXIS ULTRA DLD with an Al Kα radiation source. Binding energies (BE) are referenced to the C 1 s line 284.6 eV.

The in-situ DRIFTS experiments were performed on a Nicolet 6700 FTIR spectrometer, containing high sensitivity MCT detector which is cooled by liquid N_2 and in-situ diffuse reflectance cell (Harrick). The sample was loaded in the Harrick IR cell and heated to 350 °C for 30 min in the N_2 flow (200 mL/min) in order to remove adsorbed impurities. After preheating treatment the sample was cooled to desired reaction temperature, and at the same desired reaction temperature under N_2 atmosphere the background spectrum was collected and was subtracted from the sample spectra. The DRIFTS was recorded by accumulating 64 scans with a resolution of 4 cm^{-1}, with the total flow rate of the feeding gas was 200 mL/min. The reaction conditions were controlled as follows: 1000 ppm NH_3, 1000 ppm NO, 3% O_2 and N_2 balance if used.

2.3. Catalytic activity measurement

The fixed-bed quartz reactor with the inner diameter of 6 mm was used for SCR activity measurements. In a typical SCR experiment, 0.500 g catalyst of 40–60 meshes were used. The composition of reactant gas was as follow: 1000 ppm NH_3, 1000 ppm NO, 3% O_2 and N_2 as the balance gas, and total flow rate of the feed gas was 200 mL/min. Moreover, the corresponding gas hourly space velocity (GHSV) was 28,000 h^{-1}. In SCR reaction, the temperature was raised from 100 °C to 300 °C, and composition of the product gas was analyzed by online mass spectra (QIC-20, Hidden) for multiple species of molecule. When the catalytic reaction practically reached to a steady state flow mode (at least 40 min), the activity data was collected at their corresponding temperature. And the calibration patterns between the signal intensity and gas concentration of NO, NH_3, N_2O and NO_2 are provided in Fig. S1 in the Supplementary Information. The NO_x conversion, NH_3 conversion and N_2 selectivity were calculated according to the following Eqs. (1)–(3):

$$NO\, conversion\, =\, 100\% \times ([NO]_{in} - [NO]_{out})/[NO]_{in} \qquad (1)$$

$$NH_3\, conversion\, =\, 100\% \times ([NH_3]_{in} - [NH_3]_{out})/[NH_3]_{in} \qquad (2)$$

$$N_2\, selectivity\, =\, 100\% \times ([NO]_{in} + [NH_3]_{in} - [NO_2]_{out}$$
$$- 2[N_2O]_{out})/([NO]_{in} + [NH_3]_{in}) \qquad (3)$$

Where $[NO]_{in}$ and $[NH_3]_{in}$ refer to the inlet concentrations of NO and NH_3, respectively, $[NO]_{out}$, $[NH_3]_{out}$, $[NO_2]_{out}$ and $[N_2O]_{out}$ refer to reactor outlet concentrations of NO, NH_3, NO_2 and N_2O, respectively.

3. Results and discussion

3.1. Catalytic activity for NH_3-SCR

The effects of temperature on NO conversion were performed over the Cu_x-$Ce_{0.5-x}$-$Zr_{0.5}$ catalysts with different molar ratios of Cu/Ce, and the results are illustrated in Fig. 1(A). The catalytic activity of $Cu_{0.5}$-$Zr_{0.5}$ catalyst was very low in the temperature range of 150–270 °C. On the other hand, the $Ce_{0.5}$-$Zr_{0.5}$ catalyst only showed significant NO conversion (>60%) above 250 °C. However, the Cu_x-$Ce_{0.5-x}$-$Zr_{0.5}$ (x = 0.1, 0.2, 0.3 and 0.4) catalysts exhibited excellent activity in the temperature range of 150–270 °C. The $Cu_{0.1}$-$Ce_{0.4}$-$Zr_{0.5}$ catalyst gave nearly 100% NO conversion at 150 °C and reached up to 100% at temperature window of 170–240 °C. The $Cu_{0.2}$-$Ce_{0.3}$-$Zr_{0.5}$ catalyst displayed 100% NO conversion in a wide operation temperature window of 150–250 °C at GHSV of 28,000 h^{-1}. On further increasing the Cu amount and decreasing Ce amount, the SCR activity of the $Cu_{0.3}$-$Ce_{0.2}$-$Zr_{0.5}$ and $Cu_{0.4}$-$Ce_{0.1}$-$Zr_{0.5}$ catalysts showed lower than that of $Cu_{0.2}$-$Ce_{0.3}$-$Zr_{0.5}$ at low temperatures. When the temperature increased above 240 °C, the NO conversion decreased rapidly.

The NH_3 conversion over the Cu_x-$Ce_{0.5-x}$-$Zr_{0.5}$ samples during the tests is shown in Fig. 1(B). Below 250 °C, the NH_3 conversion was very similar with the corresponding NO conversion over each catalyst, indicating that both NO and NH_3 were consumed with the same molar ratio. Above 250 °C, the NH_3 conversion over all $Cu_{0.5}$-$Zr_{0.5}$, $Ce_{0.5}$-$Zr_{0.5}$ and Cu_x-$Ce_{0.5-x}$-$Zr_{0.5}$ catalysts kept to be 100%, which is associated with the oxidation of NH_3 in addition to SCR reaction. The N_2 selectivity was very high for all the Cu_x-$Ce_{0.5-x}$-$Zr_{0.5}$ catalysts during the whole temperature window (below 250 °C) listed in Fig. 1(C). The $Cu_{0.5}$-$Zr_{0.5}$ and $Ce_{0.5}$-$Zr_{0.5}$ showed the lowest N_2 selectivity which started to decrease at about 200 °C. For Cu_x-$Ce_{0.5-x}$-$Zr_{0.5}$ (x = 0.1, 0.2, 0.3 and 0.4), significant N_2
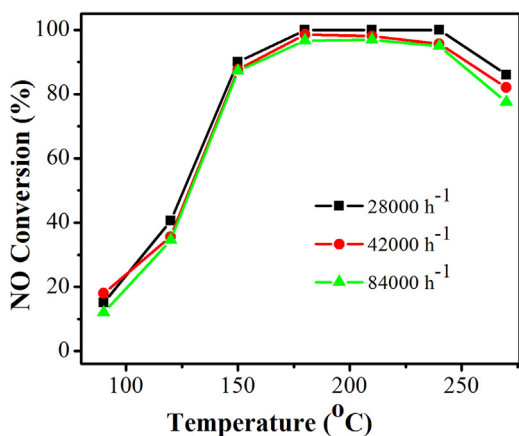
Fig. 2. Effect of GHSV on NO conversion over $Cu_{0.2}$-$Ce_{0.3}$-$Zr_{0.5}$ catalyst (Reaction conditions: [NO] = [NH_3] = 1000 ppm, [O_2] = 3%, and N_2 balance).
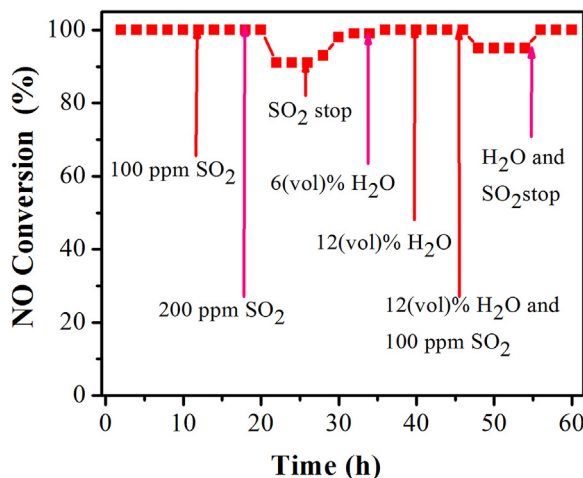
Fig. 3. Effect of SO_2, H_2O, and SO_2 + H_2O on NO conversion over the $Cu_{0.2}$-$Ce_{0.3}$-$Zr_{0.5}$ catalyst at 240 °C (Reaction conditions: [NO] = [NH_3] = 1000 ppm, [O_2] = 3 vol%, [SO_2] = 100 and 200 ppm, [H_2O] = 6 vol% and 12 vol%, and GHSV = 28,000 h^{-1}).

selectivity was observed during the whole temperature range, in which the selectivity of the $Cu_{0.2}$-$Ce_{0.3}$-$Zr_{0.5}$ catalyst was more than 95%.

3.2. Effect of GHSV

Since the $Cu_{0.2}$-$Ce_{0.3}$-$Zr_{0.5}$ displayed the excellent NO conversion and nearly 100% N_2 selectivity, thus, it was selected to systematically study the NH_3-SCR performance including the effect of different GHSV and the resistance of H_2O and SO_2.

The NO conversion over $Cu_{0.2}$-$Ce_{0.3}$-$Zr_{0.5}$ catalyst under different GHSV is displayed in Fig. 3(A). It can be seen that NO conversion below 210 °C was nearly same at different GHSV. Above 210 °C, the NO conversion slightly decreased with the increase in GHSV from 28,000 to 84,000 h^{-1}. However, the NO conversion was still more than 80% in the temperature range from 150 to 270 °C under a GHSV of 84,000 h^{-1}. In general, the effect of GHSV on the NO conversion at low temperature was weaker than that at high temperature. In order to distinguish the activity between $Cu_{0.2}$-$Ce_{0.3}$-$Zr_{0.5}$ and $Cu_{0.1}$-Ce_{04}-$Zr_{0.5}$, much higher GHSV of 84,000 h^{-1} was also selected to measure the NH_3-SCR of NO reaction over $Cu_{0.1}$-Ce_{04}-$Zr_{0.5}$ displayed in Fig. S2 in the Supplementary Information. It is noteworthy that $Cu_{0.2}$-$Ce_{0.3}$-$Zr_{0.5}$ exhibited much higher activity (Fig. 2) than $Cu_{0.1}$-Ce_{04}-$Zr_{0.5}$ (Fig. S2) under same high GHSV of 84,000 h^{-1}. These results indicate that the $Cu_{0.2}$-$Ce_{0.3}$-$Zr_{0.5}$ catalyst is a best

choice for the removal of NO in a wide temperature range from 150–270 °C even when the GHSV is as high as 84,000 h^{-1}.

3.3. Effect of SO_2 and H_2O

The SO_2 and H_2O in the exhaust usually deactivate the catalyst and consequently lower the NH_3-SCR activity [36]. Hence, better SO_2 and H_2O resistance is required for SCR process. To test the effect of H_2O and SO_2 on SCR activities, two classical procedures were applied, (i) the reaction is either performed over a wide temperature range or (ii) carried out at a given temperature [37]. It is well known that the SCR process is unable to quickly attain a stable state at low temperature, so the catalyst stability experiments toward H_2O and SO_2 performed at a given temperature is more precisely to reveal the real behavior of the catalyst [38]. The $Cu_{0.2}$-$Ce_{0.3}$-$Zr_{0.5}$ catalyst was selected to examine the SO_2 and H_2O durability and the results are presented in Fig. 3. Here, the SCR reaction was operated at 240 °C under a GHSV of 28,000 h^{-1} and the reaction was carried out for 12 h before the addition of H_2O and/or SO_2. When 100 ppm SO_2 was added to the feeds, the NO conversion showed no decrease until 6 h later and remained in stable value. The result indicates that $Cu_{0.2}$-$Ce_{0.3}$-$Zr_{0.5}$ catalyst owns excellent SO_2 tolerance, and this property is very significant for the industrial aspect of catalyst. When the catalyst was exposed to 200 ppm SO_2 for 8 h, the NO conversion decreased to 90%, and it recovered to almost 100% after the SO_2 supply was turned off. Thus, the results proposed that the $Cu_{0.2}$-$Ce_{0.3}$-$Zr_{0.5}$ catalyst was not poisoned by SO_2. It is interesting to note that 6% H_2O in the feed gas had also no prominent effect on the deNO activity of catalyst, and remained at steady value even 12% H_2O. These results indicate that the $Cu_{0.2}$-$Ce_{0.3}$-$Zr_{0.5}$ catalyst has much higher water resistance. The $Cu_{0.2}$-$Ce_{0.3}$-$Zr_{0.5}$ catalyst was exposed to both SO_2 and water vapor for 8 h and their combined effect was also examined. The results demonstrated the catalyst poisoning somewhat increase, and the NO conversion decreased to 90%. When the supply of SO_2 and water vapor was turned off, it was observed that the NO conversion restored to about 100% and remained at this stable level. The results point out that the deactivation is reversible. The SO_2/H_2O resistance of the $Cu_{0.2}$-$Ce_{0.3}$-$Zr_{0.5}$ catalyst was also conducted at 200 °C presented in Fig. S3 in the Supplementary Information. The results are similar to that at 240 °C, which indicates that the $Cu_{0.2}$-$Ce_{0.3}$-$Zr_{0.5}$ catalyst also exhibits excellent SO_2 + H_2O resistance at low temperature (200 °C).

The SO_2/H_2O resistance of the $Cu_{0.2}$-$Ce_{0.3}$-$Zr_{0.5}$ catalyst was also conducted at much higher GHSV (56,000 h^{-1}) and the results are exhibited in Fig. S4 in the Supplementary Information. The NO conversion was 98% after the introduction of 100 ppm SO_2 under GHSV of 56,000 h^{-1}, which was lower than that under GHSV of 28,000 h^{-1} in Fig. 3. When the catalyst was exposed to both 100 ppm SO_2 and 6% H_2O water vapor for 8 h and their combined effect was also evaluated, the results indicate the catalyst poisoning, and consequently the NO conversion decreased to 87%. The effect of 6% H_2O on the NO conversion at GHSV 56,000 h^{-1} and at GHSV 28,000 h^{-1} was similar. These results demonstrate that SO_2/H_2O resistance of the $Cu_{0.2}$-$Ce_{0.3}$-$Zr_{0.5}$ catalyst slightly decreases as the GHSV change from 28,000 h^{-1} to 56,000 h^{-1}. From above results, it is concluded that the $Cu_{0.2}$-$Ce_{0.3}$-$Zr_{0.5}$ catalyst exhibits excellent NH_3-SCR of NO even in the presence of SO_2 and H_2O at high GHSV.

3.4. Separated NH_3 and NO oxidation

In order to investigate the NH_3 and NO oxidation and activation, the separated NH_3 and NO oxidation experiments were conducted over the Cu_x-$Ce_{0.5-x}$-$Zr_{0.5}$ catalysts. As shown in Fig. 4(A), the NH_3 conversion over the Cu_x-$Ce_{0.5-x}$-$Zr_{0.5}$ catalysts was noticeably higher than that over $Cu_{0.5}$-$Zr_{0.5}$ and $Ce_{0.5}$-$Zr_{0.5}$, indicating that the
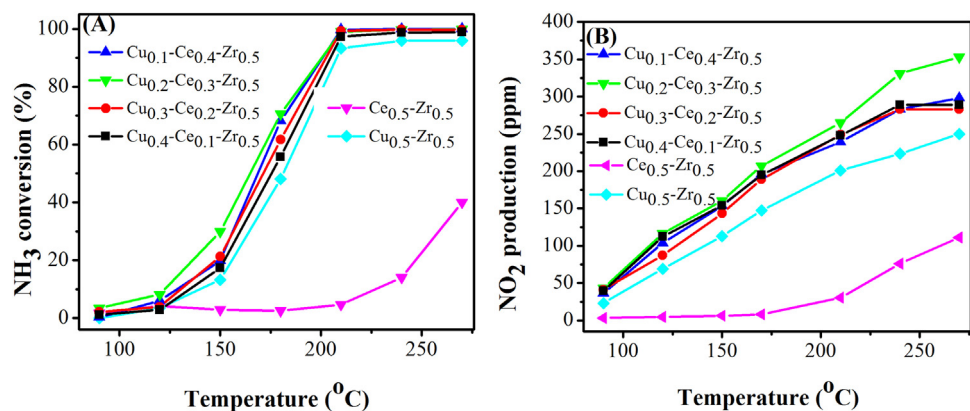
Fig. 4. (A) NH_3 conversions during separate NH_3 oxidation reaction and (B) NO_2 productions during separate NO oxidation over the Cu_x-$Ce_{0.5-x}$-$Zr_{0.5}$ ($x = 0$–0.5) catalysts (Reaction conditions: [NO] = 1000 ppm (NO oxidation test), [NH_3] = 1000 ppm (NH_3 oxidation test), [O_2] = 3%, N_2 balances, GHSV = 28,000 h^{-1}).


Fig. 5. XRD patterns of the Cu_x-$Ce_{0.5-x}$-$Zr_{0.5}$ ($x = 0$-0.5) catalysts.
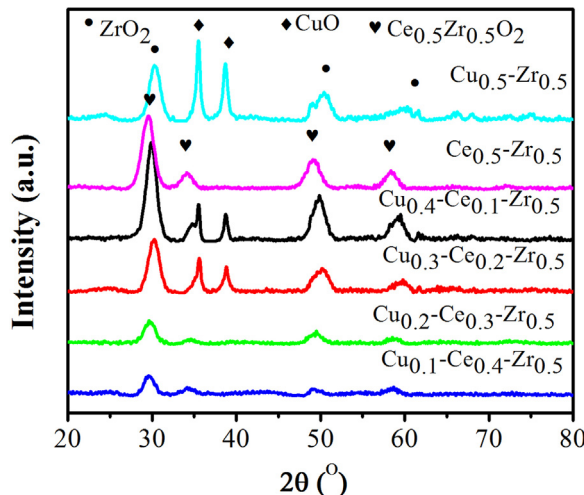

Fig. 6. Raman spectra of the Cu_x-$Ce_{0.5-x}$-$Zr_{0.5}$ ($x = 0$-0.5) catalysts.

Cu_x-$Ce_{0.5-x}$-$Zr_{0.5}$ catalysts could promote the NH_3 activation and thus beneficial for NH_3-SCR reaction. However, the NH_3 conversion was nearly 40% over the Cu_x-$Ce_{0.5-x}$-$Zr_{0.5}$ catalysts when the oxidation temperature was below 180 °C. Furthermore, it is noteworthy that the NH_3 conversion increased sharply and got to 100% at 240 °C, which suggests that the decrease in the selectivity of N_2 should be due to the NH_3 over oxidation (Fig. 1). The Fig. 4(B) depicts NO_2 production during the separated NO oxidation. According to the literatures [2,38,39], if a catalyst has the capability to completely oxidize NO to NO_2 *in situ* under NH_3-SCR conditions, then at low temperature the NO_x can be efficiently removed by accelerating the "fast SCR" process ($2NH_3 + NO + NO_2 \rightarrow 2N_2 + 3H_2O$). Our results clarify that the NO_2 production over the catalysts matched perfectly with that of the low-temperature NO_x conversion. The NO_2 production over the Cu_x-$Ce_{0.5-x}$-$Zr_{0.5}$ ($x = 0.1$-0.4) catalysts was obviously higher than that over $Cu_{0.5}$-$Zr_{0.5}$ and $Ce_{0.5}$-$Zr_{0.5}$. These results demonstrate that the Cu_x-$Ce_{0.5-x}$-$Zr_{0.5}$ ($x = 0.1$–0.4) catalysts could effectively promote the oxidation of NO during NH_3-SCR reaction and thereby enhanced the low-temperature SCR activity.

3.5. XRD and BET surface area

The XRD patterns of the Cu_x-$Ce_{0.5-x}$-$Zr_{0.5}$ ($x = 0$, 0.1, 0.2, 0.3, 0.4, 0.5) catalysts are shown in Fig. 5. The characteristic diffraction peaks of ZrO_2 (JCPDS 50-1089) and CuO (JCPDS 65-2309) were detected for the $Cu_{0.5}$-$Zr_{0.5}$ catalyst [34]. The intense XRD peaks of

CuO in $Cu_{0.5}$-$Zr_{0.5}$ catalyst indicate the presence of crystallized CuO. For the $Ce_{0.5}$-$Zr_{0.5}$ catalyst, the characteristic diffraction peaks were attributed to the $Ce_{0.5}Zr_{0.5}O_2$ phase (JCPDS 38-1436). For $Cu_{0.4}$-$Ce_{0.1}$-$Zr_{0.5}$, very interesting results were obtained. The diffraction peaks assigned to the $Ce_{0.5}Zr_{0.5}O_2$ phase were disappeared, but the diffraction peaks assigned to CuO and ZrO became prominent. With the increase in Ce/Cu ratio in the Cu_x-$Ce_{0.5-x}$-$Zr_{0.5}$ ($x = 0.1$-0.4) catalysts, the intensity of the diffraction peaks assigned to CuO and ZrO became weaker and weaker. For $Cu_{0.2}$-$Ce_{0.3}$-$Zr_{0.5}$ and $Cu_{0.1}$-Ce_{04}-$Zr_{0.5}$, only very weak diffraction peaks of ZrO and CuO were obtained. These results indicate that there is strong interaction between copper and cerium for $Cu_{0.2}$-$Ce_{0.3}$-$Zr_{0.5}$ and $Cu_{0.1}$-Ce_{04}-$Zr_{0.5}$, which leads to the high dispersion of these copper and cerium oxides and as a result formation of the complete amorphous structure [40].
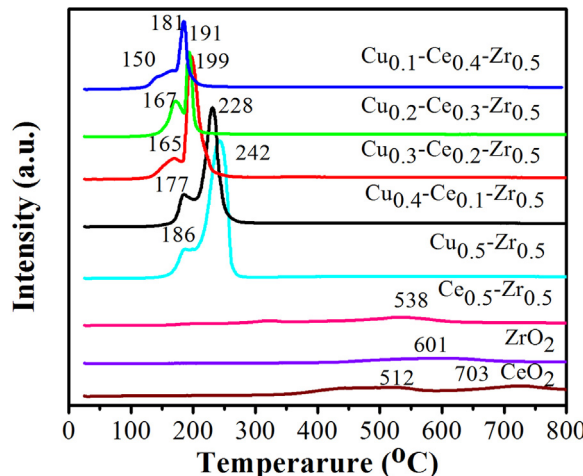
The BET surface areas of all catalysts are summarized in Table 1. Most of Cu_x-$Ce_{0.5-x}$-$Zr_{0.5}$ catalysts showed higher BET surface area than $Cu_{0.5}$-$Zr_{0.5}$ and $Ce_{0.5}$-$Zr_{0.5}$, meanwhile, the $Cu_{0.2}$-$Ce_{0.3}$-$Zr_{0.5}$ presented the largest surface area (76 $m^2 g^{-1}$), which could provide more adsorption and active sites, and consequently contributes to the excellent SCR performance to some extent.

3.6. Raman Study

In order to investigate the structure phases of the catalysts, Raman spectroscopy was carried and results are shown in Fig. 6. For $Cu_{0.5}$-$Zr_{0.5}$, five main bands were observed at 617, 429, 293,

Table 1
Physicochemical properties of the Cu_x-$Ce_{0.5-x}$-$Zr_{0.5}$ ($x = 0$-0.5) catalysts.

Samples	S_{BET} ($m^2 g^{-1}$)[a]	XPS data[b]			H_2 consumption ($\mu mol\, g^{-1}$)[c]		
		Cu^+/Cu (%)	Ce^{3+}/Ce (%)	$O_2^{\delta-}/O^{2-}$ (%)	A	β	$\alpha/(\alpha+\beta)$ (%)
$Cu_{0.5}$-$Zr_{0.5}$	65	46	–	38	13	69	15.8
$Cu_{0.4}$-$Ce_{0.1}$-$Zr_{0.5}$	69	34.4	27	56	13	61	17.6
$Cu_{0.3}$-$Ce_{0.2}$-$Zr_{0.5}$	74	40	35	61	9	54	14.3
$Cu_{0.2}$-$Ce_{0.3}$-$Zr_{0.5}$	76	50	49	77	15	21	41.7
$Cu_{0.1}$-$Ce_{0.4}$-$Zr_{0.5}$	60	46	46	70	7	21	25.0
$Ce_{0.5}$-$Zr_{0.5}$	43	–	38.3	46	–	–	–

[a] BET surface area.
[b] data calculated from XPS curves.
[c] data calculated from H_2-TPR curves.

Fig. 7. H_2-TPR profiles of the CeO_2, ZrO_2 and Cu_x-$Ce_{0.5-x}$-$Zr_{0.5}$ ($x = 0$–0.5) catalysts.

240 and 132 cm^{-1}. The broad bands at 617 and 430 cm^{-1}, weak peak at 293 cm^{-1} and medium intensity peak at 132 cm^{-1} can be attributed to the t-ZrO_2 phase [41–43]. The peak at 240 cm^{-1} can be assigned to the bulk CuO [44]. Similarly, the $Ce_{0.5}$-$Zr_{0.5}$ catalyst displays three obvious bands at 617, 450, and 132 cm^{-1} and a weak band at 290 cm^{-1}. The band at 450 cm^{-1} is ascribed to the overlap of 429 cm^{-1} assigned to t-ZrO_2 and F_{2g} mode of CeO_2 fluorite structure [44]. The two band at 132 and 617 cm^{-1} and a weak peak at 290 cm^{-1} is assigned to the Zr phase (t-ZrO_2) [42,43,45]. For $Cu_{0.4}$-$Ce_{0.1}$-$Zr_{0.5}$ and $Cu_{0.3}$-$Ce_{0.2}$-$Zr_{0.5}$, the bands assigned to CuO and t-ZrO_2 phases still exist, however, their intensity became weaker and weaker with the decrease in Cu content. When Cu content decreases to 0.2 and 0.1, the band attributed to the CuO, t-ZrO_2 and fluorite CeO_2 become very weak and almost disappear. These results demonstrate that the $Cu_{0.2}$-$Ce_{0.3}$-$Zr_{0.5}$ and $Cu_{0.1}$-$Ce_{0.4}$-$Zr_{0.5}$ catalysts are almost amorphous structure, which may be related to the interaction between Cu and Ce oxides. These results are agreement with the XRD results.

3.7. H_2-TPR measurement

H_2-TPR analysis was conducted to investigate the reducibility of the Cu_x-$Ce_{0.5-x}$-$Zr_{0.5}$ ($x = 0$–0.5) catalysts and the results are depicted in Fig. 7. Two very weak reduction peaks at low temperature (400–550 °C) and high temperature (703 °C) can be distinguished in the H_2-TPR profile of the CeO_2 catalyst, which were attributed to the reduction of surface oxygen and lattice oxygen [22,25,46], respectively. For pure ZrO_2, a hardly distinguishable peak at 601 °C can be assigned to reduction of the surface oxygen and some of the lattice oxygen of ZrO_2 [47,48]. The reduction behavior of mixed oxides was quite different from those of pure CeO_2 and ZrO_2. For $Ce_{0.5}$-$Zr_{0.5}$, the reduction peak at about 538 °C was

attributed to the reduction of surface Ce^{4+} to Ce^{3+} [49]. For $Cu_{0.5}$-$Zr_{0.5}$, a sharp peak at 242 °C with a shoulder at 186 °C was detected. Reduction of the Cu_x-$Ce_{0.5-x}$-$Zr_{0.5}$ ($x = 0.1$, 0.2, 0.3 and 0.4) catalysts was similar to that of $Cu_{0.5}$-$Zr_{0.5}$ that presented two distinct peaks, a sharp peak at higher temperature and the shoulder at lower temperature. According to the literature [50], the peak at low temperature (α peak) i.e. 177, 165, 167 and 150 °C for Cu_x-$Ce_{0.5-x}$-$Zr_{0.5}$ with the increase in x from 0.1 to 0.4 can be attributed to the reduction of high dispersed surface CuO species ($Cu^{2+} \rightarrow Cu^{+1} \rightarrow Cu^0$) [17], and corresponding peak at high temperature (β peak) i.e. 228, 199, 191 and 181 °C, can be ascribed to the reduction of small size crystalline CuO. The H_2 consumption of the reduction peak was calculated by performing a peak-fitting deconvolution using pure CuO as standard. The results are displayed in Table 1, and the corresponding fitted peak is shown in Fig. S5 in the Supplementary Information. It was noticed that the relation of the H_2 consumption of high dispersed CuO with the x value in Cu_x-$Ce_{0.5-x}$-$Zr_{0.5}$ exhibited volcano type, meanwhile, the $Cu_{0.2}$-$Ce_{0.3}$-$Zr_{0.5}$ catalyst depicted the highest H_2 consumption of the high dispersed CuO (15 $\mu mol\, g^{-1}$) and the maximum H_2 consumption ratio of α peak to (α + β) peak (α/(α + β)) (41.7%). These results indicate the presence of more high dispersed CuO and less crystalline CuO species in the $Cu_{0.2}$-$Ce_{0.3}$-$Zr_{0.5}$ catalyst, which are consistent with the XRD results. In addition, α peak shifts towards low temperature with an increase in the cerium content, indicating that the reduction of CuO species is influenced by the interaction between copper and cerium.

3.8. XPS analysis

The surface atomic concentrations and specific oxidation state of copper, cerium zirconium and oxygen on the surface of all catalysts were investigated by XPS. It is quite difficult to calculate the surface atomic concentration and discriminate the specific oxidation states of these elements without the peak deconvolution. The XPS of Cu 2p, Ce 3d and O 1s were deconvoluted into several peaks by fitting Gaussian peaks after Shirley-background subtraction to better understand the surface species and their relative intensities in different catalysts. From the area ratio of corresponding characteristic peaks, the relative atomic concentration was calculated, and their results are listed in Table 1.

The deconvoluted XPS of Cu 2p for different catalysts are displayed in Fig. 8(A). Two main peaks at about 933.7 and 953.9 eV were attributed to Cu $2p_{3/2}$ and Cu $2p_{1/2}$. The presence of shakeup satellite peaks at 942.3 and 962.7 eV revealed that both Cu^{2+} and polycrystalline Cu_2O species were present in the samples [51,52]. From these results, it can be concluded that CuO and Cu_2O species might be present on the surface of the Cu_x-$Ce_{0.5-x}$-$Zr_{0.5}$ ($x = 0.1$, 0.2, 0.3, 0.4 and 0.5) samples [53–55]. It was worthily noticed that the main peak shifted to low binding energy from 933.7 eV to 932.2 eV with the increase in Ce content in the Cu_x-$Ce_{0.5-x}$-$Zr_{0.5}$ ($x = 0.1$, 0.2,
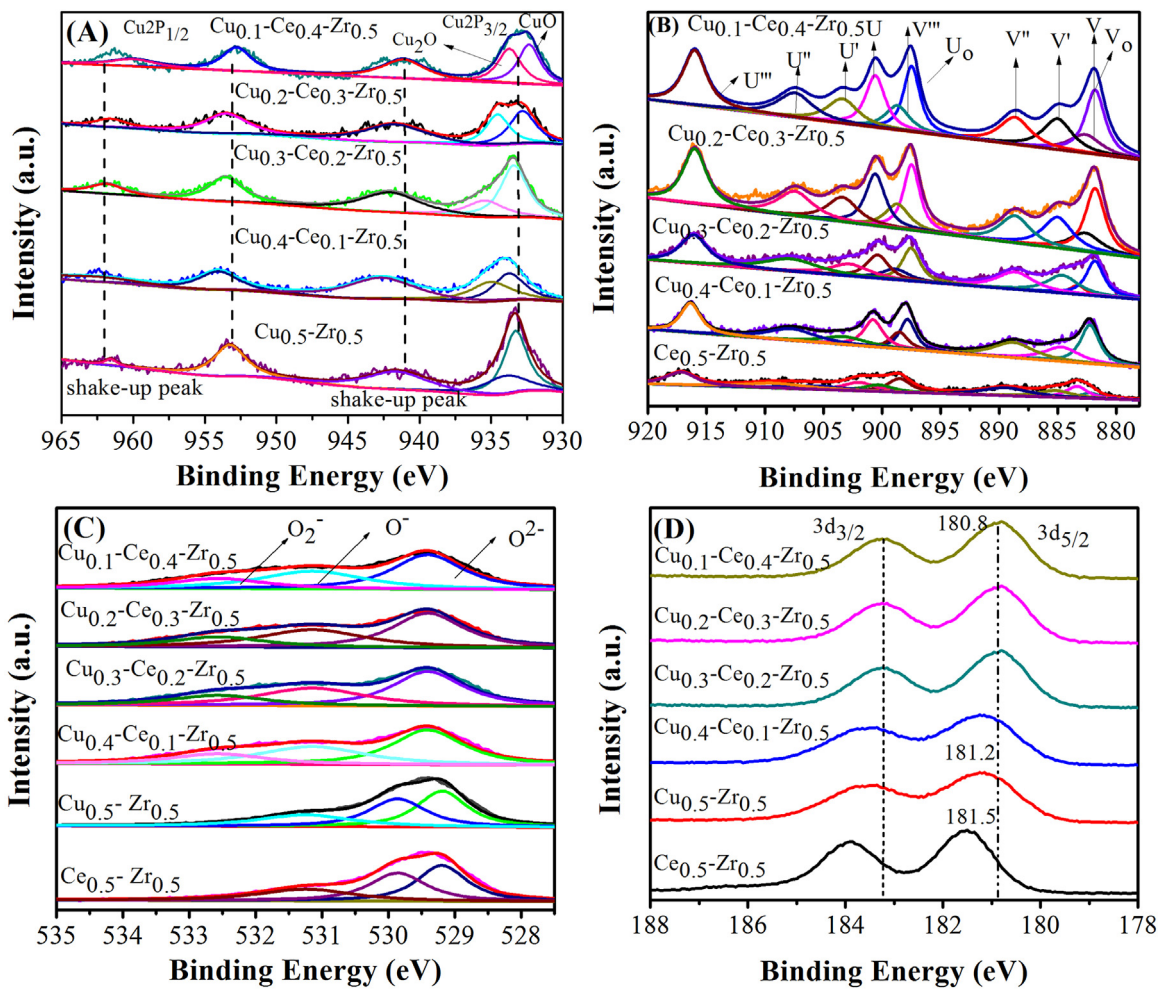
Fig. 8. XPS for (A) Cu 2p (B) Ce 3d (C) O 1s and (D) Zr 3d of the Cu_x–$Ce_{0.5-x}$–$Zr_{0.5}$ ($x = 0$-0.5) catalysts.

0.3, 0.4 and 0.5) samples. This peak shifting was attributed to the partial reduction of Cu^{2+} species to Cu^+ species [55].

The complex spectrum of Ce 3d was fitted into ten peaks with the assignment defined in Fig. 8 (B). These peaks are corresponding to five pairs of spin-orbit doublets, and were donated as V_0 (881.7 eV), V (883.2 eV), V' (884.7 eV), V'' (888.5 eV), V''' (897.3 eV), U_0 (898.4 eV), U (900.3 eV), U' (902.7 eV), U'' (907.7 eV) and U''' (916.0 eV). The peaks donated "V" represent the Ce $3d_{5/2}$ spin-orbit components and those labeled as "U" are attributed to the Ce $3d_{3/2}$ spin-orbit components [56,57]. The peaks represented by Vo, V', Uo and U' are belong to Ce^{3+} species, while those labeled as V, V'', V''', U, U'' and U''', are assigned to the characteristic peaks of Ce^{4+} species [58–61]. From Ce 3d of XPS, it is concluded that the Ce^{3+} and Ce^{4+} species are coexisted in all samples, and relative percentage of cerium species was calculated from the area ratio of Ce^{3+} to (Ce^{4+} + Ce^{3+}), and (Ce^{3+}/(Ce^{4+} + Ce^{3+}) was listed in Table 1. For $Ce_{0.5}$-$Zr_{0.5}$, the Ce^{3+}/(Ce^{4+} + Ce^{3+}) ratio is 38.3%, but the Ce^{3+}/(Ce^{4+} + Ce^{3+}) ratio increases for Cu_x-$Ce_{0.5-x}$-$Zr_{0.5}$ ($x = 0.1, 0.2, 0.3, 0.4$ and 0.5). This was probably due to that the synergic effect between Cu and Ce, which leads to some electronic interaction. The mixing of Cu and Ce together can cause a redox reaction such as $Cu^{2+} + Ce^{3+} \leftrightarrow Cu^+ + Ce^{4+}$.

The transformation of Ce^{4+} to Ce^{3+} can create the charge imbalance and oxygen vacancy on the surface, which facilitates the adsorption of oxygen species or activates reactants in the SCR reaction.

Fig. 8 (C) depicts the O 1s spectra of the different samples. The O 1s binding energies located at 529.4–529.9, 530.7–531.3 and 531.1–532.3 eV were attributed to lattice oxygen species (O^{2-}), chemisorbed oxygen species ($O_2^{\delta-}$, containing O^- and O_2^-) on oxygen vacancy sites and hydroxyl-like groups including chemisorbed water, respectively [23,62]. According to the literatures, the chemisorbed oxygen species are more reactive than the lattice oxygen in the oxidation reaction because of its higher mobility [37,57,63]. The relative concentration ratio of $O_2^{\delta-}$ to O^{2-} ($O_2^{\delta-}$/O^{2-}) over these catalysts are summarized in Table 1. The $O_2^{\delta-}$/O^{2-} ratio of $Cu_{0.2}$-$Ce_{0.3}$-$Zr_{0.5}$ is the highest among all catalysts. The results indicate that $Cu_{0.2}$-$Ce_{0.3}$-$Zr_{0.5}$ contains more chemisorbed oxygen species than the others, and thus suggesting better activity for the oxidation of NO to NO_2 at low temperature, which is in agreement with the NO oxidation results (Fig. 4 (B)).

The XPS result of Zr 3d of all sample are shown in Fig. 8 (D). The binding energy of located at range of 180.8-181.5 eV were lower than that reported for pure ZrO_2 (182.1 eV), indicating that Zr^{3+} is the main oxidation states of zirconium species for the Cu_x-$Ce_{0.5-x}$-$Zr_{0.5}$ samples [63]. Moreover, the peak positions of Zr 3d for Cu_x-$Ce_{0.5-x}$-$Zr_{0.5}$ ($x = 0.1, 0.2, 0.3$ and 0.4) shifted toward lower binding energy than that of $Cu_{0.5}$-$Zr_{0.5}$ and $Ce_{0.5}$-$Zr_{0.5}$, suggesting that partial charge shift may occur from copper and cerium species to zirconium species. Thus, according to the literature [63], it may be have the two possible reactions as follows: $Cu^+ + Zr^{4+} \leftrightarrow Cu^{2+} + Zr^{3+}$ and $Ce^{4+} + Zr^{3+} \leftrightarrow Ce^{3+} + Zr^{4+}$. However, it is well known that the

redox property between Zr^{3+} and Zr^{4+} is weak. The effect of Zr on the activity may be ignored in this study.

3.9. NH3-TPD analysis

NH_3-TPD was carried out to investigate the adsorption of NH_3 and acidity for the Cu_x-$Ce_{0.5-x}$-$Zr_{0.5}$ catalysts. The NH_3-TPD profiles of $Cu_{0.5}$-$Zr_{0.5}$, $Ce_{0.5}$-$Zr_{0.5}$ and Cu_x-$Ce_{0.5-x}$-$Zr_{0.5}$ catalysts are illustrated in Fig. 9(A). According to the literatures [36,63], the NH_3 desorption peak at low temperature was assigned to the weak acid sites. As shown in Fig. 9(A), $Cu_{0.2}$-$Ce_{0.3}$-$Zr_{0.5}$ and $Cu_{0.3}$-$Ce_{0.2}$-$Zr_{0.5}$ exhibited more acidic sites than the others based on the area of NH_3 desorption peak calculated by peak integral (Table S1 and Fig. S6A in the Supplementary Information). However, the desorption peak of $Cu_{0.2}$-$Ce_{0.3}$-$Zr_{0.5}$ located at much higher temperature than that of the other Cu_x-$Ce_{0.5-x}$-$Zr_{0.5}$ catalysts, as well as much larger peak area. These results demonstrate $Cu_{0.2}$-$Ce_{0.3}$-$Zr_{0.5}$ displays the highest acidity among the Cu_x-$Ce_{0.5-x}$-$Zr_{0.5}$ (x = 0–0.5) catalysts, which may be responsible for its distinction catalytic performance.

3.10. NO-TPD analysis

The NO-TPD results of all catalysts are given in Fig. 9(B). According to the literatures [64,65], the peaks below 250 °C can be assigned to the desorption of monodentate nitrate species, and the peaks above 250 °C were due to the decomposition of bridging nitrates species and bidentate nitrate species. Obviously, the $Ce_{0.5}$-$Zr_{0.5}$ catalyst only displayed one broad peak at about 390 °C belong to the decomposition of bridging nitrate species and bidentate nitrate species. It is noteworthy that two prominent peaks at 150–300 and 300–450 °C were observed for the Cu_x-$Ce_{0.5-x}$-$Zr_{0.5}$ (x = 0.1–0.5) catalysts, which can be assigned to desorption of monodentate nitrate species, decompose bridging nitrates species and bidentate nitrate species respectively. Among the Cu_x-$Ce_{0.5-x}$-$Zr_{0.5}$ (x = 0.1–0.5) catalysts, $Cu_{0.2}$-$Ce_{0.3}$-$Zr_{0.5}$ showed the largest peak area (Table S1 and Fig. S6 B in the Supplementary Information) especially at low temperature, indicating that NO adsorption capacity is the highest.

3.11. Synergistic effect of Cu and Ce

Above results demonstrate that the synthesized catalyst, especially $Cu_{0.2}$-$Ce_{0.3}$-$Zr_{0.5}$ display excellent NH_3-SCR activity, N_2 selectivity, stability and SO_2/H_2O durability in a broad temperature window. It is noteworthy that, the above performance was accomplished even consistent under very high GHSV, indicating that the developed low temperature SCR catalyst is promising for practical use. These results are attributed to the strong synergic effect between Cu and Ce oxides, which is addressed as follows.

It has been proved that the synergic effect caused changes in surface area, morphology, crystalline structure, surface property etc. The BET surface area of Cu_x-$Ce_{0.5-x}$-$Zr_{0.5}$ changed with mixing of Cu, Ce and Zr oxides in a different molar ratio compared with the $Ce_{0.5}$-$Zr_{0.5}$ and $Cu_{0.5}$-$Zr_{0.5}$ catalysts. Among these catalysts, the $Cu_{0.2}$-$Ce_{0.3}$-$Zr_{0.5}$ offerings the largest surface area, which could provide more adsorption and active sites, and consequently contributing to the excellent SCR performance to some extent. The XRD pattern of $Cu_{0.2}$-$Ce_{0.3}$-$Zr_{0.5}$ only displayed very weak peaks of CuO, which implies that Cu is highly dispersed and mainly present in the form of dispersed CuO. It is further confirmed by the H_2-TPR results. Where α peak area of $Cu_{0.2}$-$Ce_{0.3}$-$Zr_{0.5}$ catalyst is the highest and β peak area is the lowest among theses Cu_x-$Ce_{0.5-x}$-$Zr_{0.5}$ catalysts, indicating the presence of more dispersed CuO and less crystalline CuO species. The XRD and H_2-TPR results point out that a strong interaction does exist between Cu and Ce in the Cu_x-Ce_{5-x}-$Zr_{0.5}$ catalysts with a complete amorphous structure. The strong synergic

effect leads to more interfacial oxygen's (nested oxygen) on its surface, which is further confirmed by the XPS results. The $O_2^{\delta-}/O^{2-}$ ratio for $Cu_{0.2}$-$Ce_{0.3}$-$Zr_{0.5}$ calculated from the O 1s of XPS spectra is the highest among all the catalysts. The XPS results demonstrate that the synergic effect between Cu and Ce, which leads to the electronic interaction and cause redox reactions (Cu^{2+} + Ce^{3+} ↔ Cu^+ + Ce^{4+}) [63]. The transformation of Ce^{4+} to Ce^{3+} creating the charge imbalance and more oxygen vacancies on the surface, which is in favor of oxygen species adsorption and activation of reactants in the SCR reaction. These results indicate that $Cu_{0.2}$-$Ce_{0.3}$-$Zr_{0.5}$ possesses more chemisorbed oxygen species than the others, and thus suggesting better activity for the oxidation of NO to NO_2 at low temperature, which is confirmed by the NO oxidation results (Fig. 4(B)). It is advantage of the L-H mechanism in the SCR reaction according to the literatures [65,66]. The NO-TPD results exhibit much more adsorption amount of NO for the Cu_x-$Ce_{0.5-x}$-$Zr_{0.5}$ (x = 0.1–0.4) (Fig. 9B), which also prove the synergic effect between copper and cerium oxides. Meanwhile, $Cu_{0.2}$-$Ce_{0.3}$-$Zr_{0.5}$ gives the largest adsorption amount of NO at both low temperature and high temperature.

The surface acidity of a catalyst is one of the most important factors for NH_3-SCR reaction. The strength and amount of acid sites were critical to the adsorption of NH_3 and the followed SCR reaction cycles. NH_3-TPD results (Fig. 9A) illuminate the synergic effect between Cu and Ce oxides not only enhances the acid strength but also promotes the acid amount on the surface of catalysts, which was possibly due to the increase in the surface hydroxyl groups and charge imbalance as indicated in the XPS section. As a result, more ammonia species can participate in the SCR reaction, which could lead to the promotion of the activity of NH_3-SCR of NO. If we consider the total acidity of the catalysts, $Cu_{0.2}$-$Ce_{0.3}$-$Zr_{0.5}$ shows the highest acidity, which may be responsible for its excellent catalytic performance and N_2 selectivity [63].

Based on the results and discussion above, it can be concluded that on one hand the synergic effect between Cu and Ce oxides leads to the enhancement of electron interaction through the redox reactions of Cu^{2+} + Ce^{3+} ↔ Cu^+ + Ce^{4+}, thus, increasing the amount of active oxygen species (oxygen vacancy). On the other hand, the synergic effect also increases the acidity on the surface of catalyst, which is also beneficial to the NH_3-SCR reaction.

3.12. In situ DRIFTS studies

The above-mentioned results indicate that $Cu_{0.2}$-$Ce_{0.3}$-$Zr_{0.5}$ provides the satisfactory catalytic activity and N_2 selectivity even at high GHSV. In the following section, the reaction process of NO reduction by NH_3 over the $Cu_{0.2}$-$Ce_{0.3}$-$Zr_{0.5}$ surface was investigated with in-situ DRIFTS.

3.12.1. Adsorption of NH3/NO + O2

NH_3 adsorption on the catalysts at different time was investigated by DRIFTS, and the obtained spectra are shown in Fig. 10(A). Several bands in the range of 1150–1650 and 3100–3400 cm^{-1} were detected. The strong bands at 1615 and 1198 cm^{-1} were attributed to the σ_{as} and σ_s of NH_3 on Lewis acid sites, respectively [66–69]. The bands at 1430 cm^{-1} was assigned to the σ_s and σ_{as} of NH_4^+ on Brønsted acid sites. Several bands were observed at 3368, 3253 and 3137 cm^{-1} that was assigned to N—H region [66–69], corresponding to coordinated NH_3 on Lewis acid sites. A negative band at 3650 cm^{-1} was ascribed to the O—H groups occupied by NH_3 adsorption [70,71].

Fig. 10(B) shows the DRIFTS of NO + O_2 on the $Cu_{0.2}$-$Ce_{0.4}$-$Zr_{0.5}$ catalyst at different time. Several bands at 1177, 1240, 1548, 1580 and 1609 cm^{-1} were observed. The bands at 1580, 1177, 1240 and 1276 cm^{-1} (shoulder) were assigned to bidentate and bridged nitrate [64,66–69], while the bands at 1548 cm^{-1} were ascribed to
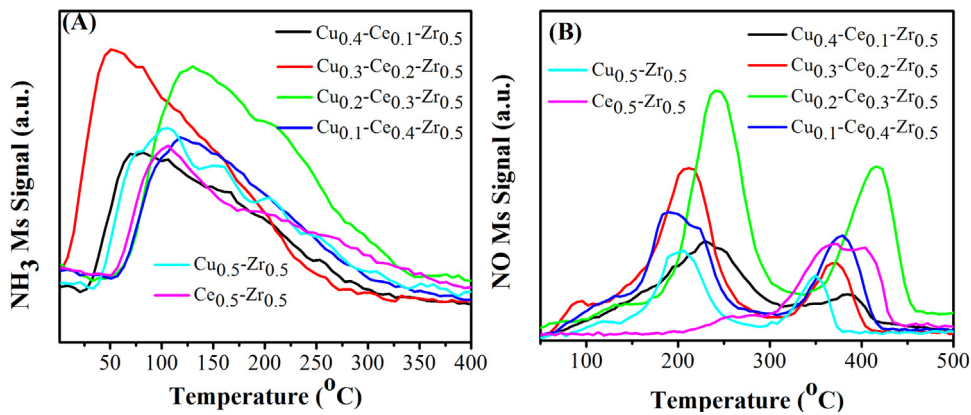
Fig. 9. (A) NH_3-TPD (B) NO-TPD profiles of the Cu_x-$Ce_{0.5-x}$-$Zr_{0.5}$ ($x = 0$–0.5) catalysts.
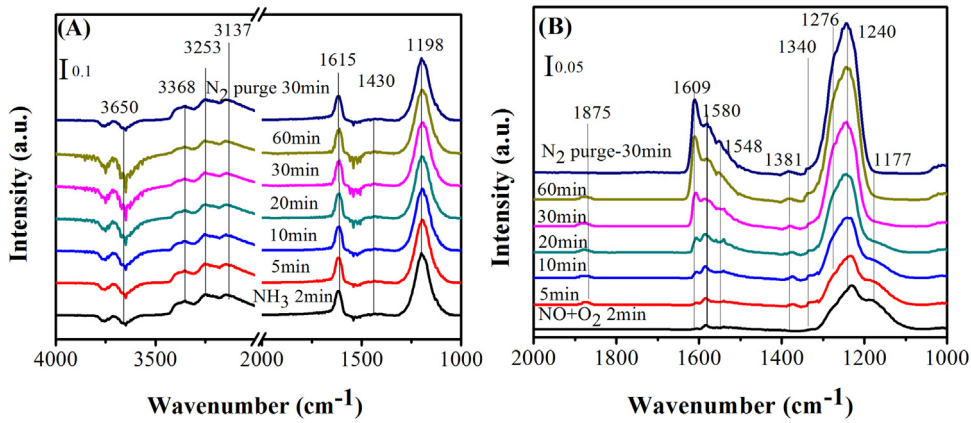
Fig. 10. DRIFTS taken at 175 °C upon passing (A) NH_3 and (B) $NO + O_2$ on the $Cu_{0.2}$-$Ce_{0.3}$-$Zr_{0.5}$ catalyst at different times.

monodentate nitrates [72,73]. The strong band at 1609 cm^{-1} was attributed to the absorbed NO_2 species [74,75] .Two weak bands at 1340 and 1381 cm^{-1} were assigned to cis-N_2O_2 [76]. The week broad band at 1875 cm^{-1} was attributed to weakly adsorbed copper mononitrosyls (Cu^{2+}-NO) [17]. It is concluded that not only presence of Lewis acid and Brønsted acid sites for the adsorption of NH_3 but also presence of many NO absorption sites are on the surface of $Cu_{0.2}$-$Ce_{0.3}$-$Zr_{0.5}$ catalyst.

3.12.2. Reaction between nitrogen oxides and adsorbed ammonia species

Reaction between nitrogen oxides and adsorbed ammonia species at 175 °C is shown in Fig. 11. First, the catalyst was exposed to NH_3 gas and followed by N_2 purging for 30 min. Then, $NO + O_2$ was introduced into the IR cell, and spectra were recorded at different interval of time. When the catalyst was treated with NH_3, the characteristic peak of coordinated NH_3 (1198 and 1615 cm^{-1}), NH_4^+ (1430 cm^{-1}) [17], and several bands of N-H at 3137, 3257 and 3350 cm^{-1} were observed [69]. These peaks disappeared quickly when the catalyst exposed to the $NO + O_2$ gas, accompanied by the appearance of new bands of NO_x (1241, 1381, 1563 and 1604 cm^{-1}) [69,71], and water (3703 cm^{-1}) [70], moreover, which became more and more intense with passage of time. The above results indicate that the absorbed NH_3 species can react with the NO_x species and be consumed after 2 min, and also it is concluded that both the coordinated NH_3 bound to Lewis acid site and NH_4^+ bound to Brønsted acid sites can participate in NH_3-SCR of NO.
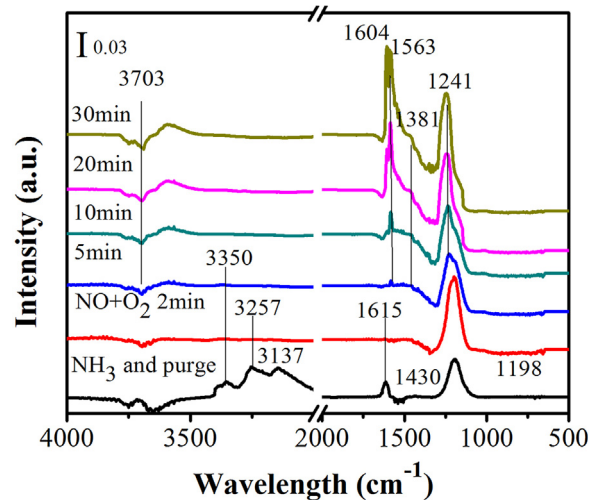

Fig. 11. DRIFTS of adsorbed species on the catalyst $Cu_{0.2}$-$Ce_{0.3}$-$Zr_{0.5}$ arising from contact with 1000 ppm NO + 5% O_2 at 175 °C (Pretreatment: 1000 ppm NH_3 preabsorbed followed by N_2 purging for 30 min).

3.12.3. Reaction between ammonia and adsorbed nitrogen oxides species

Reaction between the adsorbed nitrogen oxides species and ammonia at 175 °C is displayed in Fig. 12. First, the catalyst was exposed to the $NO + O_2$ gas and followed by N_2 purging for 30 min. Then, NH_3 was introduced into the IR cell, and spectra were recorded at different interval of time. As depicted in Fig. 12, the
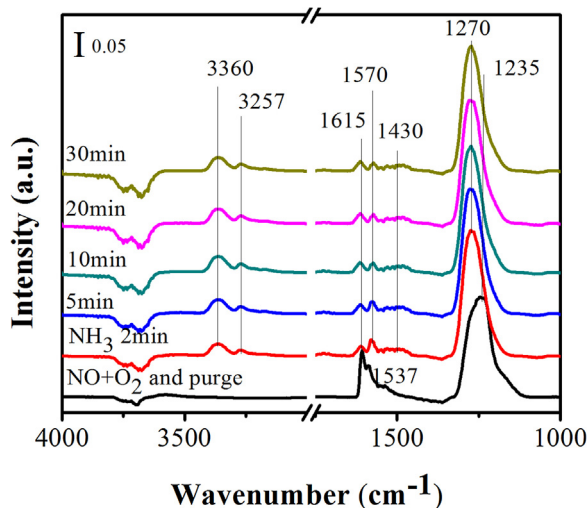
Fig. 12. DRIFTS of adsorbed species on the catalyst $Cu_{0.2}$-$Ce_{0.3}$-$Zr_{0.5}$ arising from contact with 1000 ppm NH_3 at 175 °C, N_2 balance (Pretreatment: 1000 ppm NO + 5% O_2 pre-absorbed at 175 °C followed by N_2 purging for 30 min).

Fig. 13. DRIFTS of adsorbed species arising from contact with 1000 ppm NH_3 + 1000 ppm NO + 5% O_2 at various temperatures over $Cu_{0.2}$-$Ce_{0.3}$-$Zr_{0.5.}$

peaks of monodentate nitrate (1537 cm^{-1}) [72], bridging nitrate (1235 cm^{-1}) [69], absorbed NO_2 (1609 cm^{-1}) [74,75] and bidentate nitrate (1270, 1570 cm^{-1}) [68] were prominent before NH_3 was purged into the cell. When the $Cu_{0.2}$-$Ce_{0.3}$-$Zr_{0.5}$ catalyst was exposed to the NH_3, the intensities of the bands of monodentate nitrate at 1537 cm^{-1} [71], absorbed NO_2 at 1609 cm^{-1} [74,75] and bridging nitrate at 1235 cm^{-1} [67,69] decreased rapidly and disappeared quickly after a 5 min reaction. This result demonstrates that these two kinds of nitrate species are highly reactive at low temperatures. On the other hand, the intensity of the peak attributed to bidentate nitrate (1270 and 1570 cm^{-1}) [64,68] remained unchanged even after 30 min, confirming the inactiveness of this species. After the consumption of monodenate nitrate and bridging nitrate species, a new band at about at 1430 cm^{-1} [67,68] (NH_4^+ on Bronsted acid sites), and bands at 1615, 3257 and 3360 cm^{-1} [70] (Lewis acid bonded NH_3) were appeared. Thus, the above results suggest that the absorbed NO and monodentate nitrate can react with the adsorbed NH_3 on the surface of the $Cu_{0.2}$-$Ce_{0.3}$-$Zr_{0.5}$ catalyst.

3.12.4. NH_3 + NO + O_2 co-adsorption

The DRIFTS of the $Cu_{0.2}$-$Ce_{0.3}$-$Zr_{0.5}$ catalyst following contact with NO + O_2+ NH_3 at different temperature are shown in Fig. 13. In the N—H region, several bands ascribed to coordinated NH_3 on Lewis acid sites (3360, 3265 and 3170 cm^{-1}) were detected [70]. The intense bands at 1615, 1470, 1255 and 1201 cm^{-1} were also observed, most of which could be attributed to nitrate species overlapping with σ_{as} NH_3 on Lewis acid sites at 1615 cm^{-1} [67,68]. These results indicate that most of the absorbed NH_3 species is consumed on reaction with NO_x species and the strong NO_x bands remain on the surface of the catalyst. The intense bands of coordinated NH_4^+ on Bronsted acid sites decreased at high temperatures, while the bands of coordinated NH_3 on Lewis acid sites kept unchanged even at high temperature. Thus, the coordinated NH_4^+ on the Bronsted acid sites is more active than coordinated NH_3 on Lewis acid sites at low temperature (< 200 °C), while the latter is more active for SCR at high temperature (>200 °C).

From the DRIFTS studies, it is concluded that both Lewis and Brønsted acid sites are active site for ammonia adsorption, and ammonia absorbed on catalyst surface in the form of coordinated NH_3, NH_4^+ and other NH_3 species. When NO + O_2 was passed over the NH_3-adsorbed sample, all adsorbed ammonia reacted with NO + O_2 and consumed, as a result their respective bands vanished
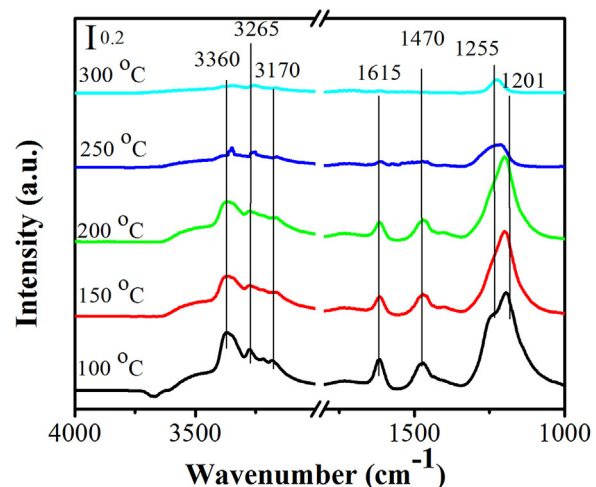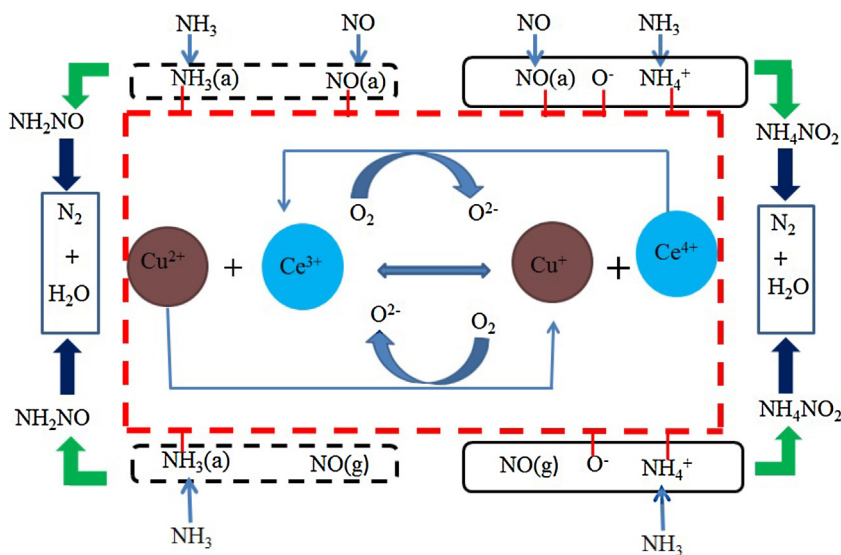
quickly (Fig. 11). After NH_3 was passed over the NO-adsorbed sample, the intensities of monodentate nitrate and bridging nitrate decreased rapidly and disappeared quickly after a 5 min reaction, while the intensity of the bidentate nitrate species very rarely changed (Fig. 12). The bands of NH_3 coordinately linked to Lewis acid sites was stable even at high temperature, where the bands of the NH_4^+ species linked to Brønsted acid sites almost vanished at high temperatures (Fig. 13).

The bands transition in (Fig. 13) suggests that the abundant amount of ionic NH_4^+ bound to Brønsted acid sites and the formation of the reactive monodenate nitrate and bridging nitrate species make important contributions to the excellent SCR performance on $Cu_{0.2}$-$Ce_{0.3}$-$Zr_{0.5}$. According to the literatures [61,68,77], the Langmuir-Hinshelwood (L-H) and Eley-Rideal (E-R) mechanisms are two most common, acceptable and widely used mechanisms for the NH_3-SCR process. A simplified reaction mechanism presented in Scheme 1 is proposed for $Cu_{0.2}$-$Ce_{0.3}$-$Zr_{0.5}$ catalyst in light of previous literatures [25,61] and our above results. According to XPS studies, the synergic effect between Cu and Ce leads to some electronic transfer, $Cu^{2+} + Ce^{3+} \leftrightarrow Cu^+ + Ce^{4+}$, increasing the amount of active oxygen species (oxygen vacancy). In addition, the synergic effect also increases the acidity on the surface of catalyst, which is also beneficial to the NH_3-SCR reaction. From DRIFT studies, it is concluded that at high temperature (above 200 °C), it is suggested that E-R mechanism is mainly followed during the reduction of NO to N_2 by NH_3. The SCR reaction occurs between gaseous NO species (NO(g)) and absorbed NH_3 species (NH$_3$(a)). During the overall SCR process, initially the absorbed NH_3 transformed to NH_2 species and in the next step it then reacts with NO(g) to form active NH_2NO/NH_4NO_2 intermediate that is extremely unstable and quickly decompose to N_2 and H_2O. The reduction of NO to N_2 by NH_3 at low temperature (below 200 °C) is considered to mainly follow the L-H mechanism, and the SCR reaction is performed between adsorbed NH_3 species and adsorbed NO species (NO(a)). The NH_3 coordinated on the Lewis acid sites and the NH_4^+ on the Brønsted acid sites can react with the adsorbed NO (L-H mechanism), as well as with gas NO (E-R mechanism) over the $Cu_{0.2}$-$Ce_{0.3}$-$Zr_{0.5}$ catalyst.

4. Conclusion

A series of Cu_x-$Ce_{0.5-x}$-$Zr_{0.5}$ catalyst prepared by citric acid method was used in the NH_3-SCR of NO reaction. The $Cu_{0.2}$-$Ce_{0.3}$-$Zr_{0.5}$ catalyst presents excellent NH_3-SCR activity in a low temperature range of 150–270 °C, along with high N_2

Scheme 1. reaction mechanism of NH$_3$-SCR over Cu$_{0.2}$Ce$_{0.3}$Zr$_{0.5}$.

selectivity, SO$_2$/H$_2$O resistance and fascinating activity at high gas hourly space velocity (GHSV) of 86,000 h^{-1}. Due to the strong interaction between copper and cerium oxides, high dispersed metal oxides are formed having adsorbed oxygen with high mobility, as a result the redox property of the Cu$_x$-Ce$_{0.5-x}$-Zr$_{0.5}$ catalyst is improved, which leads to the excellent NH$_3$-SCR activity in low temperature. The NH$_3$-TPD studies show that Cu$_{0.2}$-Ce$_{0.3}$-Zr$_{0.5}$ has the abundant acid sites which are responsible for its much higher activity and N$_2$ selectivity at low temperature. The DRIFTS studies indicate that the ionic NH$_4^+$ bound to Brønsted acid sites, coordinated NH$_3$ on the Lewis acid sites, and the active monodentate nitrate and bridging nitrate species derived from the NO$_x$ adsorption, are crucial for the SCR process. The reaction of the adsorbed NH$_3$ with the adsorbed monodentate nitrate and bridging nitrate species is responsible for the high activity of SCR reaction at low temperature. In addition, the interaction between copper and cerium creates more amounts of the surface defects over Cu$_{0.2}$-Ce$_{0.3}$-Zr$_{0.5}$, which facilitates the adsorption of oxygen species and activates the reactant in the SCR reaction.

Acknowledgements

Appendix A. Supplementary data

Supplementary data associated with this article can be found, in the online version, at http://dx.doi.org/10.1016/j.apcatb.2017.03.065.

References

[1] G. Busca, L. Lietti, G. Ramis, F. Berti, Appl. Catal. B 18 (1998) 1.
[2] J. Li, H. Chang, L. Ma, J. Hao, R.T. Yang, Catal. Today 175 (2011) 147.
[3] M.F. Irfan, J.H. Goo, S.D. Kim, Appl. Catal. B 78 (2008) 267.
[4] W. Xu, Y. Yu, C. Zhang, H. He, Catal. Commun. 9 (2008) 1453.
[5] Z. Ma, X. Wu, H. Härelind, D. Weng, B. Wang, Z. Si, J. Mole. Catal. A 423 (2016) 172.
[6] T. Zhang, R. Qu, W. Su, J. Li, Appl. Catal. B 176 (2015) 338.
[7] J. Yu, Z. Si, M. Zhu, X. Wu, L. Chen, D. Weng, J. Zou, RSC Adv. 5 (2015) 83594.
[8] S. Roy, M.S. Hegde, G. Madras, Appl. Energy 86 (2009) 2283.
[9] F. Can, X. Courtois, S. Berland, M. Seneque, S. Royer, D. Duprez, Catal. Today 257 (2015) 41.
[10] D. Nicosia, I. Czekaj, O. Kröcher, Appl. Catal. B 77 (2008) 228.
[11] Å. Kling, C. Andersson, Å. Myringer, D. Eskilsson, S.G. Järås, Appl. Catal. B 69 (2007) 240.
[12] S. Ding, F. Liu, X. Shi, H. He, Appl. Catal. B 180 (2016) 766.
[13] M. Stanciulescu, G. Caravaggio, A. Dobri, J. Moir, R. Burich, J.-P. Charland, P. Bulsink, Appl. Catal. B 123 (2012) 229.
[14] Z. Si, D. Weng, X. Wu, J. Yang, B. Wang, Catal. Commun. 11 (2010) 1045.
[15] C. Zhou, Y. Zhang, X. Wang, H. Xu, K. Sun, K. Shen, J. Colloid Interface Sci. 392 (2013) 319.
[16] Z. Si, D. Weng, X. Wu, J. Li, G. Li, J. Catal. 271 (2010) 43.
[17] L. Chen, Z. Si, X. Wu, D. Weng, ACS Appl. Mater. Interface 6 (2014) 8134.
[18] J.A. Sullivan, J.A. Doherty, Appl. Catal. B 55 (2005) 185.
[19] X. Gao, Y. Jiang, Y. Fu, Y. Zhong, Z. Luo, K. Cen, Catal. Commun. 11 (2010) 465.
[20] E. Ito, Y. Mergler, B. Nieuwenhuys, H. Van Bekkum, C. Van den Bleek, Microporous Mater. 4 (1995) 455.
[21] T. Gu, Y. Liu, X. Weng, H. Wang, Z. Wu, Catal. Commun. 12 (2010) 310.
[22] P. Li, Y. Xin, Q. Li, Z. Wang, Z. Zhang, L. Zheng, Environ. Sci. Technol. 46 (2012) 9600.
[23] W. Shan, F. Liu, H. He, X. Shi, C. Zhang, Appl. Catal. B 115 (2012) 100.
[24] W. Shan, F. Liu, H. He, X. Shi, C. Zhang, Catal. Today 184 (2012) 160.
[25] Z.P. Zhang, L.Q. Chen, Z.B. Li, P.Y. Li, F.L. Yuan, X.Y. Niu, Y.J. Zhu, Catal. Sci. Technol. 6 (2016) 7151.
[26] X. Gao, X. Du, L. Cui, Y. Fu, Z. Luo, K. Cen, Catal. Commun. 12 (2010) 255.
[27] X. Du, X. Gao, L. Cui, Z. Zheng, P. Ji, Z. Luo, K. Cen, Appl. Surf. Sci. 270 (2013) 370.
[28] R. Guo, W. Zhen, W. Pan, Y. Zhou, J. Hong, H. Xu, Q. Jin, C. Ding, S. Guo, J. Ind. Eng. Chem. 20 (2014) 1577.
[29] X. Jiang, P. Lu, C. Li, Z. Zeng, G. Zeng, L. Hu, L. Mai, Z. Li, Electron. Technol. 34 (2013) 591.
[30] X. Gao, X. Du, L. Cui, Y. Fu, Z. Luo, K. Cen, Catal. Commun. 12 (2010) 255.
[31] X. Li, M. Shen, X. Hong, H. Zhu, F. Gao, Y. Kong, L. Dong, Y. Chen, J. Phys. Chem. B 109 (2005) 3949.
[32] E. Moretti, L. Storaro, A. Talon, M. Lenarda, P. Riello, R. Frattini, M.V.M. Yuso, A. Jiménez-López, E. Rodríguez-Castellón, F. Ternero, A. Caballero, J.P. Holgado, Appl. Catal. B 102 (2011) 627.
[33] L. Liu, Y. Chen, L. Dong, J. Zhu, H. Wan, B. Liu, B. Zhao, H.Y. Zhu, K.Q. Sun, L. Dong, Y. Chen, Appl. Catal. B 90 (2009) 105.
[34] Y. Shen, Y. Ma, S. Zhu, Catal. Sci. Technol. 2 (2012) 589.
[35] P.Y. Li, F.L. Yuan, D. Wang, Y.L. Dong, X.Y. Niu, Y.J. Zhu, Catalysis 6 (2016) 124.
[36] K.J. Lee, P.A. Kumar, M.S. Maqbool, K.N. Rao, K.H. Song, H.P. Ha, Appl. Catal. B 142 (2013) 705.
[37] H. Xu, Q. Zhang, C. Qiu, T. Lin, M. Gong, Y. Chen, Chem. Eng. Sci. 76 (2012) 120.
[38] G. Qi, R.T. Yang, Appl. Catal. B 44 (2003) 217.
[39] F. Liu, W. Shan, Z. Lian, L. Xie, W. Yang, H. He, Catal. Sci. Technol. 3 (2013) 2699.
[40] P.R. Ettireddy, N. Ettireddy, T. Boningari, R. Pardemann, P.G. Smirniotis, J. Catal. 292 (2012) 53.
[41] B.M. Reddy, P. Lakshmanan, A. Khan, J. Phys. Chem. B 108 (2004) 16855.
[42] S. Gao, X. Chen, H. Wang, J. Mo, Z. Wu, Y. Liu, X. Weng, J. Colloid Interface Sci. 394 (2013) 515.
[43] S. Letichevsky, C.A. Tellez, R.R. de Avillez, M.I.P. da Silva, M.A. Fraga, L.G. Appel, Appl. Catal. B 58 (2005) 203.

[44] V.R.K. Chary, G.V. Sagar, D. Naresh, K.K. Seela, B. Sridhar, J. Phys. Chem. B 109 (2005) 9437.
[45] S. Ding, F. Liu, X. Shi, K. Liu, Z. Lian, L. Xie, H. He, ACS Appl. Mater. Interfaces 7 (2015) 9497.
[46] G. Neri, A. Pistone, C. Milone, S. Galvagno, Appl. Catal. B 38 (2002) 321.
[47] S. Esposito, M. Turco, G. Bagnasco, C. Cammarano, P. Pernice, A. Aronne, Appl. Catal. A 372 (2010) 48.
[48] V.R. Choudhary, B.S. Uphade, S.G. Pataskar, Appl. Catal. A 227 (2002) 29.
[49] Z. Wu, H. Zhu, Z. Qin, H. Wang, L. Huang, J. Wang, Appl. Catal. B 98 (2010) 204.
[50] L. Xiaowei, S. Mingmin, H. Xi, Z. Haiyang, G. Fei, K. Yan, D. Lin, C. Yi, J. Phys. Chem. B 109 (2005) 3949.
[51] C.C. Chusuei, M. Brookshier, D. Goodman, Langmuir 15 (1999) 2806.
[52] S. Andonova, E. Vovk, J. Sjöblom, E. Ozensoy, L. Olsson, Appl. Catal. B 147 (2014) 251.
[53] T. Boningari, D.K. Pappas, P.R. Ettireddy, A. Kotrba, P.G. Smirniotis, Ind. Eng. Chem. Res. 54 (2015) 2261.
[54] F. Marquez, A. Palomares, F. Rey, A. Corma, J. Mater. Chem. 11 (2001) 1675.
[55] L. Martin, H. Martinez, D. Poinot, B. Pecquenard, F. Le Cras, J. Phys. Chem. C 117 (2013) 4421.
[56] L. Zhang, D. Zhang, J. Zhang, S. Cai, C. Fang, L. Huang, H. Li, R. Gao, L. Shi, Nanoscale 5 (2013) 9821.
[57] F. ç. Larachi, J. Pierre, A. Adnot, A. Bernis, Appl. Surf. Sci. 195 (2002) 236.
[58] N. Perret, X. Wang, J.J. Delgado, G. Blanco, X. Chen, C.M. Olmos, S. Bernal, M.A. Keane, J. Catal. 317 (2014) 114.
[59] L.E. Gómez, E.E. Miró, A.V. Boix, Int. J. Hydrogen Energy 38 (2013) 5645.
[60] K.N. Rao, P. Venkataswamy, B.M. Reddy, Ind. Eng. Chem. Res. 50 (2011) 11960.
[61] B. Guan, H. Lin, L. Zhu, Z. Huang, J. Phys. Chem. C 115 (2011) 12850.
[62] L. Chen, J. Li, M. Ge, J. Phys. Chem. C 113 (2009) 21177.
[63] X. Zhao, L. Huang, H. Li, H. Hu, X. Hu, L. Shi, D. Zhang, Appl. Catal. B 183 (2016) 269.
[64] Z. Lian, F. Liu, H. He, X. Shi, J. Mo, Z. Wu, J. Chem. Eng. 250 (2014) 390.
[65] F. Liu, H. He, Y. Ding, C. Zhang, Appl. Catal. B 93 (2009) 194.
[66] M.A. Larrubia, G. Ramis, G. Busca, Appl. Catal. B 30 (2001) 101.
[67] G. Ramis, L. Yi, G. Busca, M. Turco, E. Kotur, R.J. Willey, J. Catal. 157 (1995) 523.
[68] L. Chen, J. Li, M. Ge, Environ. Sci. Technol. 44 (2010) 9590.
[69] M.A. Larrubia, G. Ramis, G. Busca, Appl. Catal. B 27 (2000) L145.
[70] D. Sun, Q. Liu, Z. Liu, G. Gui, Z. Huang, Appl. Catal. B 92 (2009) 462.
[71] G. Ramis, L. Yi, G. Busca, Catal. Today 28 (1996) 373.
[72] D. Wang, L. Zhang, K. Kamasamudram, W.S. Epling, ACS. Catal. 3 (2013) 871.
[73] S. Brandenberger, O. Kröcher, A. Wokaun, A. Tissler, R. Althoff, J. Catal. 268 (2009) 297.
[74] Y. Liu, T. Gu, X. Weng, Y. Wang, Z. Wu, H. Wang, J. Phys. Chem. C 116 (2012) 16582.
[75] Y.H. Yeom, B. Wen, W.M. Sachtler, E. Weitz, J. Phys. Chem. C B 108 (2004) 5386.
[76] M. Machida, M. Uto, D. Kurogi, T. Kijima, J. Mater. Chem. 11 (2001) 900.
[77] G. Qi, R.T. Yang, R. Chang, Appl. Catal. B 51 (2004) 93.